Phytomedicine 65 (2019) 153102

Contents lists available at ScienceDirect

Phytomedicine

journal homepage: www.elsevier.com/locate/phymed

Original Article

Effect of *Euphorbia* factor L1 on intestinal barrier impairment and defecation dysfunction in *Caenorhabditis elegans*

Zhu An[a], Ji Zonghui[a], Zhao Jingwei[a], Zhang Wenjing[b,c], Sun Yuqing[a], Zhang Tao[a], Gao Shan[b], Li Guojun[b,c,**], Wang Qi[a,d,e,*]

[a] Department of Toxicology, School of Public Health, Peking University, Beijing 100191, China
[b] Beijing Key Laboratory of Diagnostic and Traceability Technologies for Food Poisoning, Beijing Center for Disease Prevention and Control, Beijing Center of Preventive Medicine Research, Beijing 100013, China
[c] School of Public Health, Capital Medical University, Beijing 100069, China
[d] Key Laboratory of State Administration of Traditional Chinese Medicine for Compatibility Toxicology, Beijing 100191, China
[e] Beijing Key Laboratory of Toxicological Research and Risk Assessment for Food Safety, Beijing 100191, China

ARTICLE INFO

Keywords:
Euphorbia factor L1
Caenorhabditis elegans
Oxidative stress
Intestinal permeability
Defecation behavior
γ-aminobutyric acid

ABSTRACT

Background: *Euphorbia* factor L1 (EFL1) is a lathyrane-type diterpenoid from the medicinal herb *Euphorbia lathyris* L., and has been reported with intestinal toxicity, but the potential mechanisms remain unknown.
Purpose: The objective of this study was to investigate the intestinal toxicity of EFL1 and the underlying mechanisms using nematode *Caenorhabditis elegans*.
Methods: *C. elegans* were exposed to 0–200 μM EFL1 for 72 h, then the survival rate, body length and body width, locomotion and chemoreception behavior, intestinal ROS and lipofuscin accumulation, intestinal permeability, and defecation rhythm were detected. The γ-aminobutyric acid (GABA) energic neurons AVL and DVB were shown *via* green fluorescent protein under a laser scanning confocal microscope. The structure of GABA transporter UNC-47 were predicted by homology modeling, and the interaction between EFL1 and UNC-47 was simulated by molecular docking. The mRNA expression of genes related to oxidative stress, intestinal permeability and defecation after EFL1 exposure were detected by RT-qPCR.
Results: EFL1 did not induce lethality of nematodes. The general toxicity was characterized by abnormal growth, locomotion and chemoreception. The intestinal barrier was leaky, due to down-regulated cell junction and active cation transport. The mean defecation cycle length in nematodes was decreased, relating to disorder vesicular and ion transport, enhanced rhythm behavior and muscle contraction. The dysfunctional defecation also attributed to injured UNC-47 protein, as well as GABAergic neurons AVL and DVB. Excessive ROS and lipofuscin accumulation were observed in intestine, along with activation of antioxidant enzymes of SOD, COQ7 and CAT.
Conclusion: This study elucidated the EFL1-induced intestinal toxicity in nematodes, characterized as leaky intestinal barrier and accelerated defecation behavior. The underlying mechanisms were involved in oxidative stress, cell junctions, transportation, rhythm behavior, muscle contraction, and GABAergic neurons.

Introduction

Euphorbia semen is the seed of *Euphorbia lathyris* L. (*Euphorbiaceae*), and has been clinically used to treat hydropsy, ascites, amenorrhea, anuria and constipation in traditional Chinese medicine (TCM) (Zhang et al., 2019). Totally 33 kinds of lathyrane-type diterpenoids have been isolated from *E. lathyris*, of which *Euphorbia* factor L1 (EFL1) has a mass percent of ≥0.35% (w/w). In recent years, EFL1 has

Abbreviations: CAT, catalase; DCFH-DA, 2′7′-dichlorofluorescin diacetate; EFL1, *Euphorbia* factor L1; Emc, enteric muscle contraction; GABA, γ-aminobutyric acid; GFP, green fluorescent protein; H_2O_2, hydrogen peroxide; NGM, nematode growth medium; ROS, reactive oxygen species; SOD, superoxide dismutase; TCM, traditional Chinese medicine

* Correspondence to Wang Qi: Department of Toxicology, School of Public Health, Peking University, No. 38 Xueyuan Road, Haidian District, Beijing 100191, China.
** Correspondence to Li Guojun: Beijing Key Laboratory of Diagnostic and Traceability Technologies for Food Poisoning; Beijing Center for Disease Prevention and Control; Beijing Center of Preventive Medicine Research, Hepingli middle street 16, Dongcheng District, Beijing 100013, China.
E-mail addresses: ligj@bjcdc.org (G. Li), wangqi@bjmu.edu.cn (Q. Wang).

https://doi.org/10.1016/j.phymed.2019.153102
Received 21 May 2019; Received in revised form 22 September 2019; Accepted 26 September 2019
0944-7113/

attracted increased attention for its efficacy to inhibit adipogenesis and reverse multidrug resistance, possessing prospects in anti-obesity and oncotherapy (Gao et al., 2007).

Clinically, *Euphorbia* semen has intestinal adverse effect manifested by hyperemesis and diarrhea, and EFL1 is identified as the main toxic ingredient (Zhu et al., 2018). Previous studies have demonstrated the cytotoxicity of EFL1 in several kinds of cells (Zhang et al., 2011). Recently, the toxicity of EFL1 was further examined in mice, reporting pathologic lesion in colon and defective intestinal barrier (Wang et al., 2018). However, the information about the toxicity of EFL1 is still insufficient. Especially, we know little about its intestinal toxicity effect and mechanism.

The laboratorial researches generally use rodents to explore intestinal toxicity, expending enormous amount of time and money. The nematode *Caenorhabditis elegans*, a free-living coelomic organism, has emerged as excellent model in toxicological research, due to simplicity of maintenance, short life cycle, small body size and large brood size. Additionally, *C. elegans* was the first multicellular organism whose whole-genomic sequencing was elucidated. Around 60–80% homologues of human genes had been identified, depending on the different bioinformatics approach used (Harris et al., 2004). It is convenient to explore the gene mechanisms of toxicant. *C. elegans* has been used for the toxicity assessment of environmental pollutants and drugs, and has been applied in several studies to assay the adverse effects of toxic ingredients from medicinal herb (Xia et al., 2018).

The intestinal toxicity is reflected as inflammation, edema, abnormal defecation in humans, and evaluated by reactive oxygen species (ROS), lipofuscin, permeability and defecation behavior in *C. elegans*. At physiological condition, ROS act as signaling molecules to regulate development, adaptation and survival of nematodes, but hyperactive aerobic metabolism will generate excessive ROS, and cause oxidative damage to functional units of DNA, protein and lipids (Jazwinski, 1996). Lipofuscin, a not degradable fluorochrome product of lipid peroxidation, will accumulate in lysosome and cannot be excreted by exocytosis. The *C. elegans* defecation is a highly coordinated rhythmic behavior regulated by γ-aminobutyric acid (GABA) energic neurons that synapse onto the enteric muscles (Mahoney et al., 2008). Injured GABAergic neurons and dysfunctional defecation were observed in toxic xenobiotics-exposed *C. elegans* (Zhao et al., 2016).

In the present study, we used the model organism *C. elegans* to study the intestinal toxicity effects of EFL1, including the role of oxidative stress, permeability and defecation. The underlying toxicity mechanisms were investigated *via* analysis of gene expression and GABAergic neurons. *In silico* methods of homology modeling and molecular docking, as well as *in vivo* studies of behavior, fluorescent imaging and neurodevelopment, were performed to explore EFL1-induced intestinal impairment.

Materials and methods

Chemical reagents

EFL1 (the chemical stucture as shown in Fig. 1A) was purchased from Spring and Autumn Biological Engineering Company (Nanjing, China), and had a purity of 98.75% as previously described (Zhu et al., 2019). The fluorescent dye 2,7-dichlorofuorescin diacetate (DCFH-DA) was obtained from Solarbio (Beijing, China). Dimethyl sulfoxide (DMSO) and sodium azide (NaN_3) were obtained from Amresco (Solon, OH, USA). Irinotecan was obtained from TargetMol (Wellesley Hills, MA, USA). All the other chemicals were obtained from Sigma-Aldrich (St. Louis, MO, USA), except as otherwise noted.

Strain preparation and EFL1 exposure

Nematodes used in this study were wide-type Bristol N2, and transgenic strain of *oxIs*12[Ex(P*unc-47::GFP*)], originally obtained from *Caenorhabditis* Genetics Center (CGC, Minneapolis, MN, USA). They were maintained on nematode growth medium (NGM) plates seeded with *E. coli* OP50 at 20 °C as previously described (Brenner, 1974), and OP50 during EFL1 exposure were inactivated by ^{60}Co radiation at dose of 10 KGy to avoid the potential drug metabolism by bacteria (Ji et al., 2019). Gravid hermaphrodite nematodes were washed off from the plates into conical tubes, and were lysed by bleaching mixture buffer (0.45 M NaOH, 2% HOCl). Age synchronous populations of L1-larvae nematodes were obtained as described (Donkin and Williams, 1995).

Exposure to EFL1 were performed from L1-larvae to young adult for 72 h (see Fig. 1B) in a 24-well plates at 20 °C in the presence of inactivated OP50. During exposure, nematodes were added into sterile S medium containing 100 mM NaCl, 5.74 mM K_2HPO_4, 44 mM KH_2PO_4, 10 μM potassium citrate, 3 μM $CaCl_2$, 3 μM $MgSO_4$, 1.29 μM cholesterol and some trace metal. EFL1 was dissolved in DMSO, and the final working concentrations of EFL1 were 12.5, 25, 50, 100 and 200 μM. The final working concentration of DMSO was 1%, without significant effect on the development of *C. elegans* (Spence et al., 1982).

General toxicity

Lethality and growth assays

For the lethality assay, a 200 μl aliquot of test solution was added into each well of a 96-well plate, which was subsequently loaded with

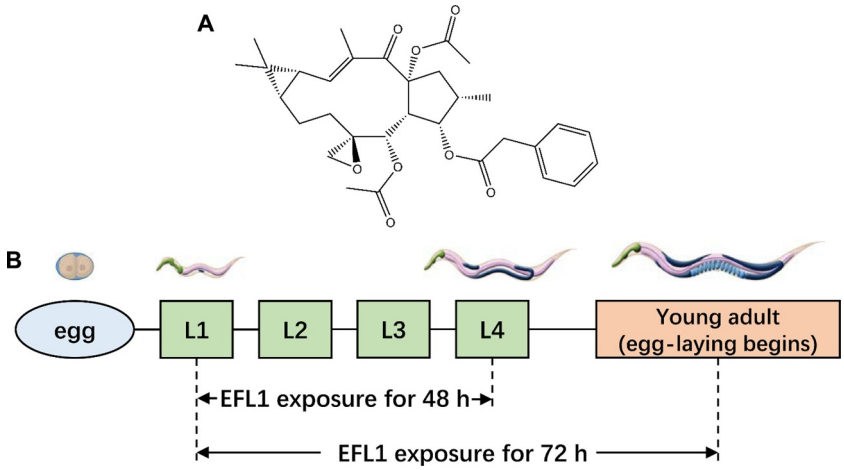

Fig. 1. (A) The chemical structure of EFL1. (B) Schematic diagram of EFL1 exposure from L1-larvae to L4-larvae or young adult in *C. elegans*.

50 nematodes for each treatment. After exposed to 0, 12.5, 25, 50, 100 and 200 μM EFL1 for 72 h, nematodes were observed under a dissecting microscope (Olympus, Tokyo, Japan), and inactive ones were recorded. Nematodes were judged to be dead if they did not respond to stimuli using a small, metal sire. Assays were performed in triplicate.

Growth was assessed by the body length and body width, which was determined by measuring flat surface area of nematodes using ZEN 2 pro software (Chinese Academy of Sciences, Shanghai, China). Twenty nematodes were examined *per* treatment, and assays were performed in triplicate.

Locomotion behavior assay

The frequencies of head thrash and body bend were determined to evaluate the locomotion behavior. A head thrash was defined as a change in the direction of bending at mid-body. A body bend was defined as a change in direction along the *Y* axis of the part of the nematodes corresponding to the posterior bulb of the pharynx, assuming that nematodes travel along the *X* axis (Wu et al., 2015). Nematodes were transferred into a new plate without food, then 60 μl M9 buffer (1 mM $MgSO_4$, 5 mM KH_2PO_4, 20 mM Na_2HPO_4 and 20 mM NaCl) was added on the agar. After 1 min recovery period, the head thrashes and body bends were recorded for 20 s. Twenty nematodes were examined *per* treatment, and assays were performed in triplicate.

Avoidance and chemotaxis assay

To examine nematodes response to $CuSO_4$ stimulus, we used the quadrant method with some modifications (Wang, 2019). The nematodes were washed twice with K medium (32 mM KCl and 51 mM NaCl) and placed on the control quadrant of the 9 cm NGM plates (Fig. 4A) partitioning into four regions with or without 0.1 M $CuSO_4$. After 90 min, the numbers of nematodes over the repellent and control areas were counted. The avoidance index was calculated as N_{CuSO4} / N_{total}, where N_{CuSO4} was the number of nematodes over the repellent area and N_{total} was the total number of nematodes on the plate. Assays were performed in triplicate.

The nematodes are usually attracted to butanedione when they are cultured on normal NGM. The chemotaxis assay was carried out according to the method previously described (Bargmann and Horvitz, 1991). Two marks were made on the back of the 9 cm NGM plate at opposite sides. Then 1 μl 1% (v/v) butanedione, together with 1 μl sodium azide were added on the agar over one mark, and 1 μl sodium azide was added over the other mark as control (Fig. 4B). The nematodes to be assayed were equidistant from the two marks. After 6 h, The numbers of nematodes over chemoattractant and control areas were counted. The chemotaxis index was calculated as ($N_{butanedione}$ − $N_{control}$) / N_{total}, where $N_{butanedione}$ and $N_{control}$ were the numbers of nematodes over the chemoattractant area and control area, respectively. Assays were performed in triplicate.

Intestinal permeability assay

The intestinal barrier function assay was performed based on the method previously described (Gelino et al., 2016). Briefly, after exposed to EFL1 for 72 h, nematodes were collected and washed twice with M9 buffer, then suspended for 3 h in blue food dye of 2.5% (w/v) erioglaucine disodium salt (Acros Organics, Morris, NJ, USA) in the presence of OP50. Subsequently, nematodes were transferred onto NGM plates seeded with OP50 to analyze the presence or absence of the blue food dye in the body cavity using a microscope (Zeiss, Oberkochen, Germany). Irinotecan, a well-known drug that induces intestinal impairment, was used in this assay as positive drug.

Pharyngeal pumping rate and mean defecation cycle length

The pharyngeal pumping rate reflected the food intake ability of *C. elegans*. The present study recorded the pharynx pumping frequency every 30 s at room temperature. The mean defecation cycle length was defined as the interval between the initiations of two successive posterior body-wall muscle contraction (Ruan et al., 2016). Twenty nematodes were examined *per* treatment, and assays were performed in triplicate.

Intestinal oxidative damage

Intestinal ROS accumulation. The oxidation-sensitive fluorescence probe 2′,7′-dichlorofluorescein diacetate (DCFH-DA) was used to measure the levels of ROS in *C. elegans*. After EFL1 exposure for 72 h, nematodes were collected and incubated with 10 μM DCFH-DA for 30 min at 20 °C in the dark, then washed twice with M9 buffer. Nematodes were mounted on 2% agar pads and anaesthetized by sodium azide to visualize intestinal ROS with laser scanning confocal microscope (Nikon, Tokyo, Japan) with 488 nm excitation wavelength and 525 nm emission filter. Images were analyzed by ZEN 2 pro software (Chinese Academy of Sciences). Twenty nematodes were examined *per* treatment, and assays were performed in triplicate. For the positive control, 0.03% hydrogen peroxide (H_2O_2) was used in this assay.

Intestinal lipofuscin levels

After exposed to 0, 12.5, 25, 50, 100 and 200 μM EFL1 for 72 h, nematodes were mounted onto 2% agar pads and anaesthetized by sodium azide to visualize intestinal autofluorescence. Images were collected using 525 nm bandpass filter at constant exposure time to preserve the relative intensity of the fluorescence of different nematodes (Wu et al., 2013). Images were obtained by Axio Imager M2 microscope (Zeiss), and lipofuscin levels were measured using ZEN 2 pro software. Twenty nematodes were examined *per* treatment, and assays were performed in triplicate.

Homology modeling and molecular docking

The structure of *C. elegans* UNC-47, a vital protein regulated defecation behavior, was predicted by homology modeling in iterative threading assembly refinement (I-TASSER) server, an integrated platform for automated protein structure prediction based on the sequence-to-structure paradigm (Yang et al., 2015). Briefly, the FASTA format amino acid sequence of UNC-47 was retrieved from UniProtKB database, and was uploaded to I-TASSER server to generate three dimensions (3D) structure model, based on multiple threading alignments and iterative structural assembly simulations. Confidence score (C-score) is used to assess the accuracy of global structure model based on the significance of threading template alignments and the convergence parameters of the structure assembly simulations. C-score is typically in range of [−5, 2], and a higher value indicates more confident prediction. The accuracy of each residue is assessed by the distance deviation between residue positions in the model and the native structure *via* ResQ method, taking into consideration the structural variations of the simulation trajectories, and homology-based data-mining (Yang et al., 2016). Normalized B-factor is used to assess the extent of the inherent thermal mobility of residues in protein, and residues with normalized B-factor ≤ 0 were more stable in protein structure.

To predict whether EFL1 could interact with UNC-47, molecular docking was performed in Surflex-Dock Geom mode of SYBYL-X 2.0 software (Tripos, St Louis, MO, USA). The energy of EFL1 was minimized *via* the addition of Gasteiger-Hückel charges in the Tripos force field. To prepare UNC-47 protein, we repaired the side chain, fixed the side chain amides, and added the hydrogen atoms. The total score, a comprehensive evaluation of hydrophobic complementarity, polar complementarity, solvation terms, and entropic terms, indicates a stable interaction when the value is higher than 5.

Fluorescent images of neurons regulating defecation behavior

Defecation is regulated by GABAergic AVL neuron in head and DVB neuron in tail in nematodes. The fluorescent images of AVL and DVB neurons regulating defecation behavior were captured with a laser scanning confocal microscope (Nikon), with 488 nm excitation wavelength and 507 nm emission filter. The relative sizes of fluorescent area

for cell bodies of AVL and DVB neurons were measured by Image-Pro Plus software (Media Cybernetics, Rockville, MD, USA). Twenty nematodes were examined *per* treatment, and assays were performed in triplicate.

Quantitative real-time polymerase chain reaction (RT-qPCR)

RT-qPCR was performed to detect the expression of genes potentially related to toxic damage. Total RNA from nematodes was isolated by using TRIzol reagent (Invitrogen, Carlsbad, CA, USA); then cDNA was synthesized from 10 μl of total RNA by using a reverse transcriptase

Table 1
Gene descriptions and sequences of qRT-PCR primers in *C. elegans*.

	Gene	Gene descriptions	Designed RT-qPCR primer sequences (5′ to 3′)	
			Forward	Reverse
Locomotion	*unc-2*	ortholog of human CACNA1; involves in locomotion	CAACGCTCAGGAACTCAC	AATCAGAACTCGGAATGG
	vav-1	ortholog of human VAV; involves in positive regulation of locomotion	GTAATGGAGGATGTCTGC	TATAGCGTTGCTTAGGTT
Chemoreception	*egl-30*	ortholog of human GNAQ; involves in chemosensory behavior	AAGAGCTATGGGAGGATT	CACCAGGAACATGATTGA
Oxidative stress	*sod-1*	ortholog of human *sod-1*; intracellular Cu/Zn-dependent SOD	ACGCTCGTCACGCTTTAC	TCTTCTGCCTTGTCTCCG
	sod-2	ortholog of human *sod-2*; mitochondrial Mn-dependent SOD	GGCATCAACTGTCGCTGT	ACAAGTCCAGTTGTTGCC
	sod-3	ortholog of human *sod-2*; mitochondrial Mn-dependent SOD	TGACATCACTATTGCGGT	GGGACCATTCCTTCCAAA
	sod-4	ortholog of human *sod-3*; extracellular Cu/Zn -dependent SOD	CACCAGATGACTCGAACA	AATGAGGCAAGAGAGTCG
	mev-1	ortholog of human SDHC; exhibits heme binding activity	GGAATTCGCTTCTTAGGAT	GCAGTCTTGTTGCTCTTGT
	isp-1	ortholog of human UQCRFS1	GCAGAAAGATGAATGGTCC	CAGAAGCGTCGTAGTGAGA
	clk-1	ortholog of human COQ7	CACATACTGCTGCTTCTCGT	TGAACCAACAGATGAACCTT
	ctl-1	ortholog of human CAT	CTCCTACACGGACACGCAT	GCATCTCCCTGGCTTTCAT
	ctl-2	ortholog of human CAT	CGAACAGCTTCAACTATGG	GTGGCTGGGAATGTGGTAT
	ctl-3	ortholog of human CAT	TTCTCCTACACGGACACGC	GCATCTCCCTGGCTTTCAT
Intestinal development	*ajm-1*	ortholog of human C9orf172; involves in apical cell-cell junction	GTCAATCAGTTCGTCCCG	ACTCGTCCGATGGTGTCT
	let-413	ortholog of human SCRIB; involves in cell-cell junction assembly	TTGCGTCCAACAAGTTAC	CACCAAGAAATGCTCCTC
	par-3	ortholog of human PARD3; involves in cell adhesion	AAGCGTAACTGTCAACCA	CCGTCTATAACATCCTCC
	egl-8	ortholog of human PLCB4; has phosphatidylinositol phospholipase C activity	GCTCGATGGCTTCAAGTA	TGAATGCTATCCCTCTGC
	ifb-2	ortholog of human LMNB2; has structural molecule activity	TCAAGGCTGAATACGACA	TCCAAAGCAGAGTTACGG
	erm-1	ortholog of human EZR; has structural molecule activity	TCCACGACTCCGTATCAA	TCCTGCTCGGCAATCTTA
	dlg-1	ortholog of human DLG; involves in zonula adherens assembly	TTGAAACGGCGTAAAGAT	CGTGATGAACTGGTGGTG
	eps-8	ortholog of human EPS; has actin filament binding activity	ACGCAGTGACGGTAGAAG	AGCGGATACACGGATACA
	nfm-1	ortholog of human NF2; has actin binding activity	ATTACGGAGGATCTGGTA	TCATCGTCGTGAACTTAT
	act-5	involves in microvillus assembly	GGGAGTGATGGTCGGTAT	CGGTAAGGAGAACTGGGT
	abts-4	ortholog of human SLC4; has inorganic anion exchanger activity	CTCAGACTACAGGGATGG	GTGCCTGACTCACAAGAC
	pkc-3	ortholog of human PRKC; has protein serine/threonine kinase activity	CGTCTCCGACATCATTAG	CAACTCGGCTTCTTGACT
	mtm-6	ortholog of human MTMR; has phosphatase binding activity	AAAAGGGACGCTAACAGC	ATTCTCAAACGCAAGCAG
	vha-6	ortholog of human ATP6V0 subunit; has H^+ transmembrane transporter activity	ATGGAGGCAAACTTAGAG	TTCCGAGATTGACATAGC
	gtl-1	ortholog of human TRPM	CTGCTCACCACGCACAAT	AACTCCTTCATCCAACCC
	pgp-1	ortholog of human ABCB; has efflux transmembrane transporter activity	AATGTCCGATTCGCTTAC	CTCAGGGTTCAACGTCTT
	inx-3	has gap junction hemi-channel activity	CAGTGGGTGCCTATTGTG	GACCGTATTCGTTCTTGG
Pharyngeal pumping	*unc-13*	ortholog of human UNC13A; regulates pharyngeal pumping	AGTGAGCCGCTTTCTTAT	AATCCTCCACCACTTTCA
	unc-36	ortholog of human CACNA2; involves in locomotion and pharyngeal pumping	CTCGCCACTTATGTCTCC	TCTTCAACTCGGCTCTTG
Defecation	*fat-3*	ortholog of human FADS; has stearoyl-CoA 9-desaturase activity	ACTCATCACGCTGCCACA	TACCCAAGCCCAATGTCC
	unc-101	ortholog of human AP1M1; involved in apical protein localization	CGGAAATTGTTGGAAGCG	CGGGCGGTATGAAGGAGA
	unc-44	ankyrin-like protein	TCCCAGACGGATCACTTA	ATTCCACGGTTGTTACTT
	unc-16	ortholog of human MAPK8IP3	CTCGGTGCTGATCTCACA	GCGTCTTAATCTCCTCCT
	shn-1	ortholog of human SHANK2; involved in defecation and rhythmic behavior	AGGAGGAAAGGTCAACGG	GTCGGAACGGCCTAGAAT
	flr-4	has protein kinase activity, involves in defecation cycle	TCCACCAGTCATTCATCG	CAGAACCTCAGGAGCCAC
	crt-1	ortholog of human CALR; has calcium ion binding activity	CTGTGGAGGTGGATACGT	GTCGGAGTTGAGGATGAG
	tax-6	ortholog of human PPP3C; has calcium ion binding activity	TGGAAAGATGGCAAGAGC	CGTTTGTCGTGACGGAAT
	egl-36	ortholog of human KCNC; involves in ion transmembrane transport	TGCCAGTTCCTGTTATCG	CTCCTAACCCTCCCTGTG
	exp-2	involvesin potassium ion transmembrane transport	GCGGCATATTGGTGGTGT	TTGCTCGCTTTGCTGGTC
	aex-5	involves in defecation and muscle contraction	AATGTGCTGGATTGGTAG	GCAATGCTCCATTCTTAA
	sup-9	ortholog of human KCNK; involved in regulation of muscle contraction	GAAGATGAACGGAGGGAT	CTTTCTGTGACGGTGTCG
	hlh-8	ortholog of human TWIST; involves in DNA binding and protein dimerization	GTCAAAGGACCAAGGAAC	TGAAAGCCGACTGTAAAT
	lim-6	ortholog of human LMX1; has DNA-binding activity transcription factor activity	GTTCTGGTTGTGGGTGTC	ATAGCATTTGATGGTCGT
	rho-1	ortholog of human RHOC; has GTP binding activity	ATTGAAGTTGACGGAAAG	TAATCGGAACATTTGGAC
GABA	*gat-1*	Na^+/Cl^--dependent GABA transporter 1	AAAGTGTAGCCGAAGTAG	AACTCGTCAATGATAGCG
	unc-25	ortholog of human GAD2; involves in GABA biosynthesis	CGGCTCAACTGTCTACGG	TGGAGAAGTGCTCCCATG
	cab-1	ortholog of human NPDC1; involves in chemical synaptic transmission	AATGCCGCTGTCAAGGAT	GTCTGCATCGCACTTTCG
	aex-3	ortholog of human MADD; involves in chemical synaptic transmission	ATTACTGGGCGATGGGTG	TGGCGAACGAGTGGATTG
	unc-33	ortholog of human DPYSL; involves in axon guidance and neuron projection	CTCCCTGACAGACGATAA	CAGACTCCGCTAACCCTA

CACNA1: calcium voltage-gated channel subunit alpha 1; **VAV**: vav guanine nucleotide exchange factor; **GNAQ**: G protein subunit alpha q; **Cu**: copper; **Zn**: zinc; **SOD**: superoxide dismutase; **Mn**: manganese; **SDHC**: succinate dehydrogenase complex subunit C; **UQCRFS1**: ubiquinol-cytochrome c reductase, Rieske iron-sulfur polypeptide 1; **COQ7**: coenzyme Q biosynthesis protein 7; **CAT**: catalase; **SCRIB**: scribbled planar cell polarity protein; **PARD3**: par-3 family cell polarity regulator; **PLCB4**: phospholipase C beta 4; **LMNB2**: lamin B2; **EZR**: ezrin;**DLG**: discs large homolog; **EPS**: Epidermal growth factor receptor kinase substrate; **NF2**: neurofibromin 2; **SLC4**: solute carrier family 4; **PRKC**: protein kinase C; **MTMR**: myotubularin related protein; **ATP6V0**: ATPase H^+ transporting V0; **TRPM**: transient receptor potential cation channel subfamily M; **ABCB**: ATP binding cassette subfamily B member; **UNC13A**: unc-13 homolog A; **CACNA2**: calcium voltage-gated channel auxiliary subunit alpha 2; **FADS**: fatty acid desaturase; **AP1M1**: adaptor protein-1 complex subunit mu-1; **MAPK8IP3**: C-jun-amino-terminal kinase-interacting protein 3; **SHANK2**: SH3 and multiple ankyrin repeat domains 2; **CALR**: Calreticulin; **PPP3C**: protein phosphatase 3 catalytic; **KCNC**: potassium voltage-gated channel subfamily C; **KCNK**: potassium two pore domain channel subfamily K member; **TWIST**: twist family bHLH transcription factor; **LMX1**: LIM homeobox transcription factor 1; **RHOC**: ras homolog C; **GABA**: γ-aminobutyric acid; **GAD2**: Glutamate decarboxylase 2; **NPDC1**: Neural proliferation differentiation and control protein 1; **MADD**: MAP kinase activating death domain; **DPYSL**: Dihydropyrimidinase-related protein 2.

reaction. The primers were synthesized as shown in Table 1, with *tba-1* used as the endogenous control. To quantify the relative mRNA expression, RT-qPCR was performed using a 20 μl reaction volume, and relative mRNA expression was calculated by the $2^{-\Delta\Delta Ct}$ method (Schmittgen and Livak, 2008) and the fold change was normalized to that observed in the control group.

Statistical analysis

The data were analyzed by using SPSS software (IBM, New York, NY, USA) and expressed as the mean ± standard error of the mean (SEM). One-way analysis of variance was performed, and the differences between the two groups were determined by the least-significant difference or Dunnett's T3 test, varied with the heterogeneity of variance. Values of $p < 0.05$ or $p < 0.01$ were considered statistically significant.

Results

Effects of EFL1 on the survival and growth of C. elegans

We tested the general toxicity in nematodes exposed to 12.5, 25, 50, 100 and 200 μM EFL1 for 72 h, but no induction of lethality were observed as shown in Fig. 2A. Subsequently, the growth of *C. elegans* exposed to EFL1 was assessed. After exposed to 100 and 200 μM EFL1 for 48 h, the body length decreased from 512.1 μm of control to 474.3 and 447.7 μm ($p < 0.01$); the body width decreased from 21.3 μm of control to 19.3 and 18.6 μm ($p < 0.01$) (Fig. 2B). For 72 h exposure, the body length decreased from 877.0 μm of control to 820.2 and 825.7 μm ($p < 0.01$), and each exposure group showed a significant decrease in body width ($p < 0.01$) (Fig. 2C).

Effects of EFL1 on the locomotion behavior of C. elegans

The locomotion behavior of *C. elegans* was evaluated by frequencies of head thrash and body bend. As shown in Fig. 3A, after EFL1 exposure for 72 h, the frequencies of body bends increased from 8.0 of control to 9.2, 9.5 and 9.9 of the 50, 100 and 200 μM EFL1 groups ($p < 0.01$). The frequencies of head thrash increased from 38.3 of control to 42.8 and 44.1 of the 100 and 200 μM EFL1 groups ($p < 0.01$).

Moreover, we investigated the effects of EFL1 exposure on the expression patterns of genes required for the regulation of locomotion behavior. Exposure to 200 μM of EFL1 for 72 h significantly increased the expression levels of *unc-2* and *vav-1* to 3.82- and 4.34-fold of control ($p < 0.05$). These two genes encode orthologs of human calcium voltage-gated channel subunit alpha 1 (CACNA1) and guanine nucleotide exchange factor (VAV) respectively, both of which positively regulate locomotion behavior.

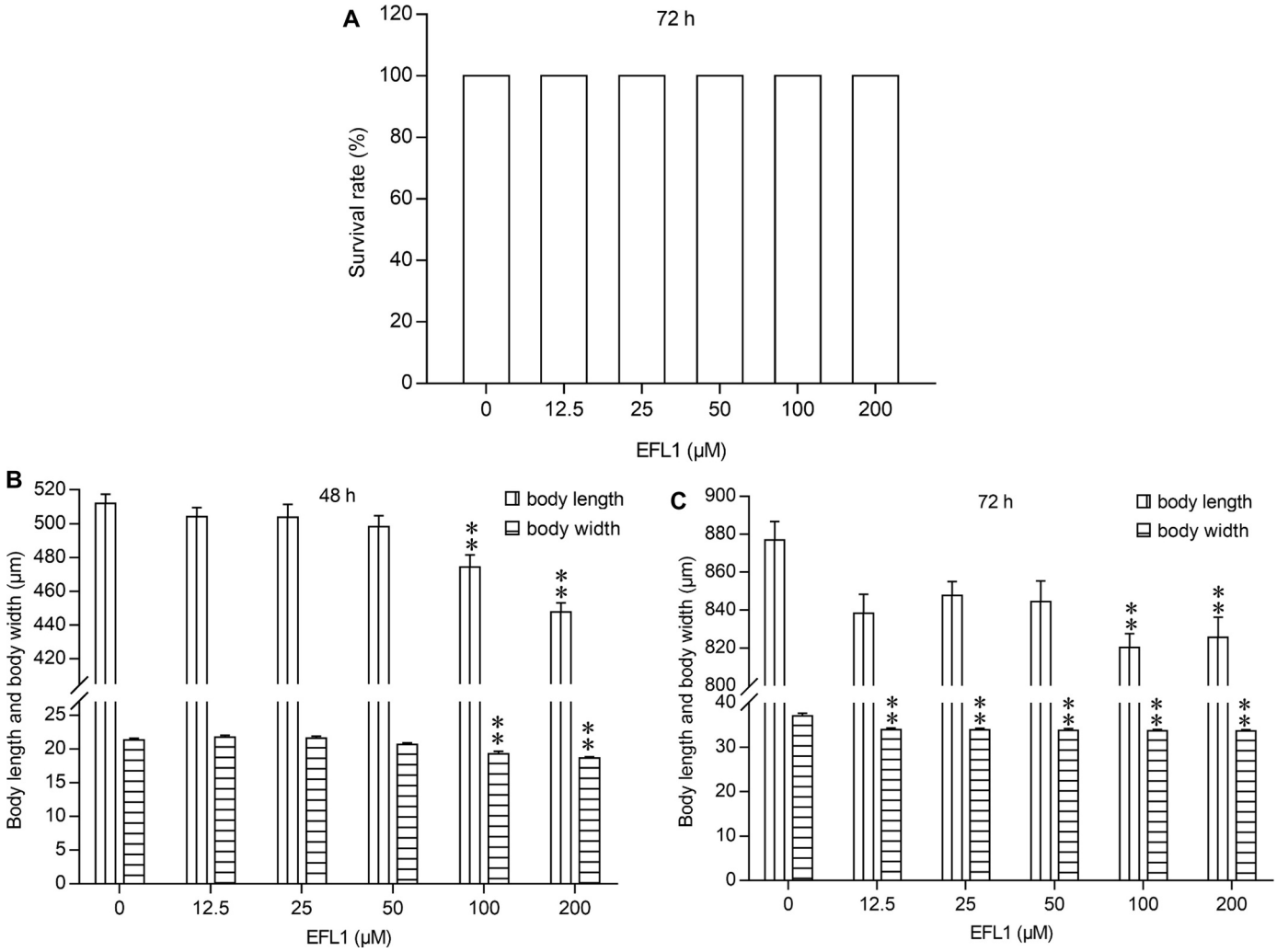

Fig. 2. (A) Effects of EFL1 exposure on lethality of *C. elegans*. (B and C) Effects of EFL1 exposure on body length and body width of *C. elegans*. Data were presented as mean ± SEM. of three independent experiments. *$p < 0.05$ or **$p < 0.01$ indicated a statistically significant difference when compared to the control.

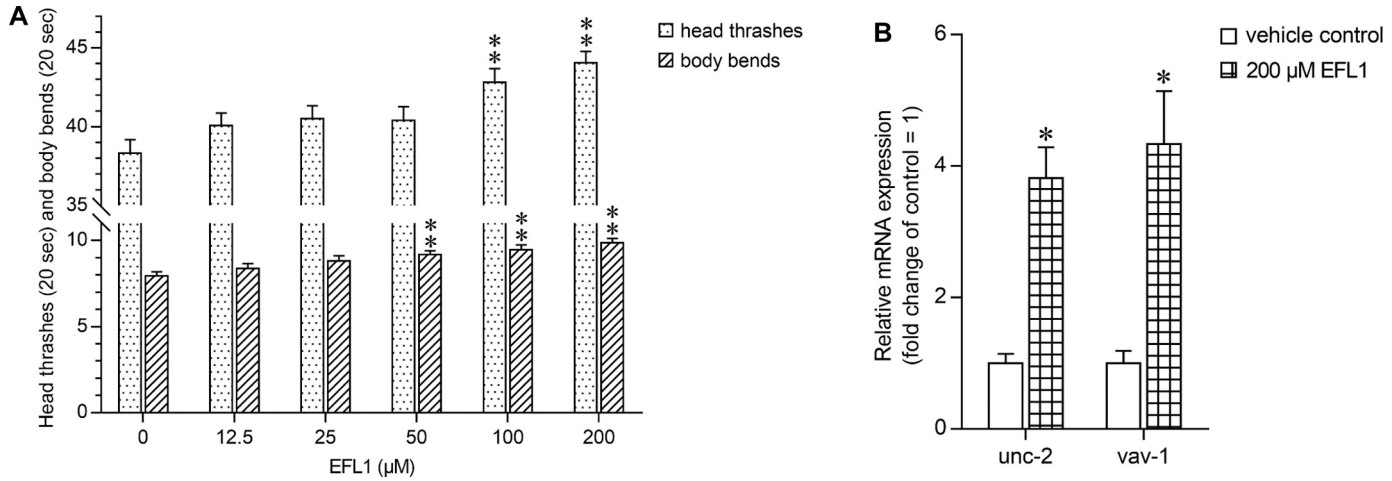

Fig. 3. Effects of EFL1 exposure on locomotion behavior in *C. elegans*. (A) The frequencies of head thrashes and body bends in 20 s. (B) Expression pattern comparison of genes required for locomotion in *C. elegans*, the results were expressed as the relative expression *ratio* between targeted genes and *tba-1* reference gene. Data were presented as mean ± SEM. of three independent experiments. $*p < 0.05$ or $**p < 0.01$ indicated a statistically significant difference when compared to the control.

Effects of EFL1 on the chemoreception of C. elegans

We examined the possible adverse effects of EFL1 exposure on the chemoreception of *C. elegans*, based on their avoidance and chemotaxis. As shown in Fig. 4C, the avoidance increased from 0.04 of control to 0.13 of 200 μM EFL1 group ($p < 0.05$), suggesting avoidance deficiency induced in high concentration EFL1 group. To the chemotaxis index, 12.5–200 μM concentrations of EFL1 did not induce significant change compared to the control.

Gene *egl-30* encodes ortholog of human G protein subunit alpha q (GNAQ), and is involved in the regulation of chemosensory behavior. In the present study, the mRNA expression level of *egl-30* was detected, with the result of decreasing to 63.50% of control ($p < 0.05$). The results suggested that EFL1-induced avoidance deficiency may related to the down-regulation of *egl-30*.

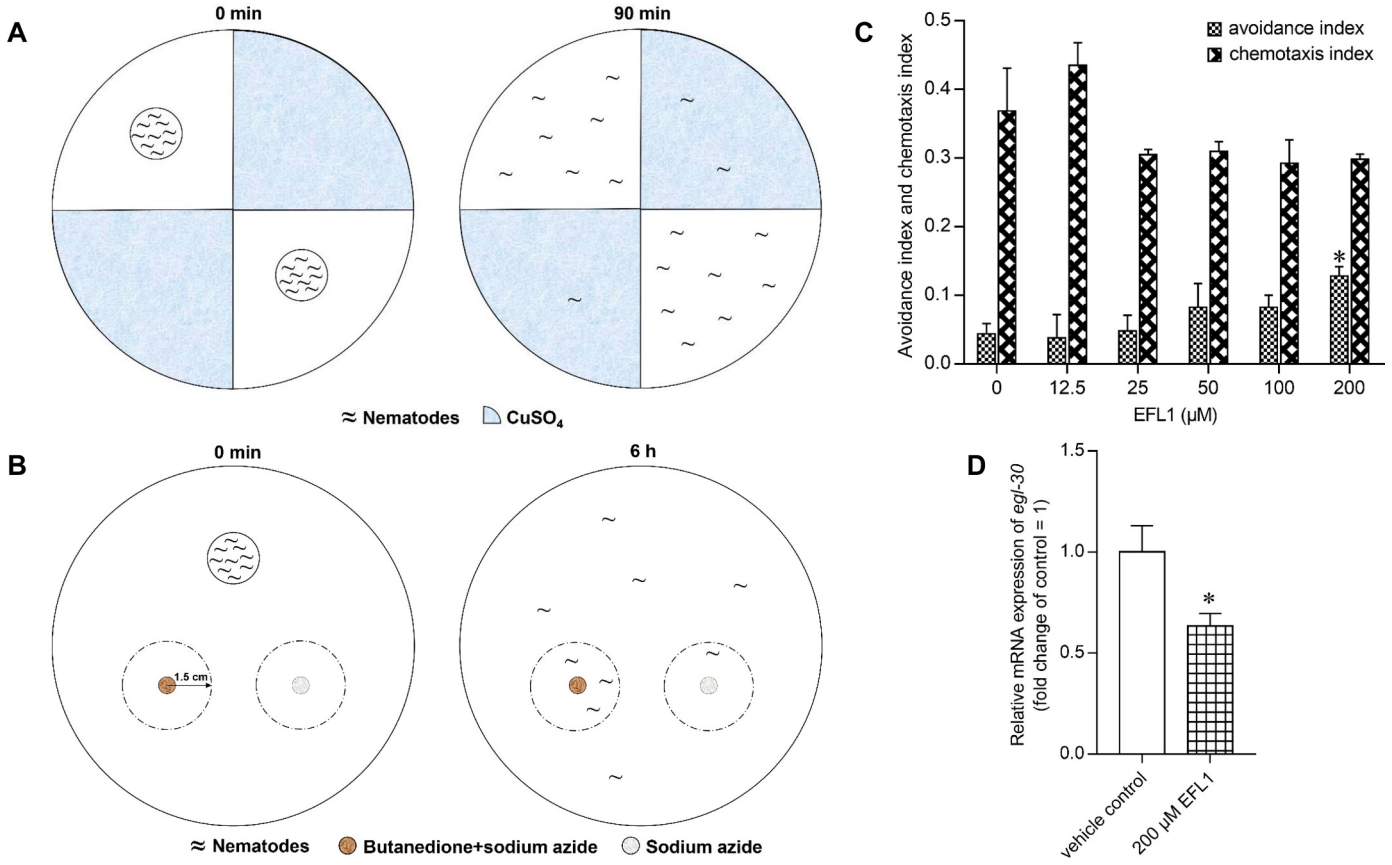

Fig. 4. (A) Schematic diagram for the avoidance assay. (B) Schematic diagram for the chemotaxis assay. (C) Effects of EFL1 exposure on the avoidance index and chemotaxis index in *C. elegans*. (D) The *egl-30* gene expression change in *C. elegans*, the results were expressed as the relative expression *ratio* between *egl-30* gene and *tba-1* reference gene. Data were presented as mean ± SEM of three independent experiments. $*p < 0.05$ or $**p < 0.01$ indicated a statistically significant difference when compared to the control.

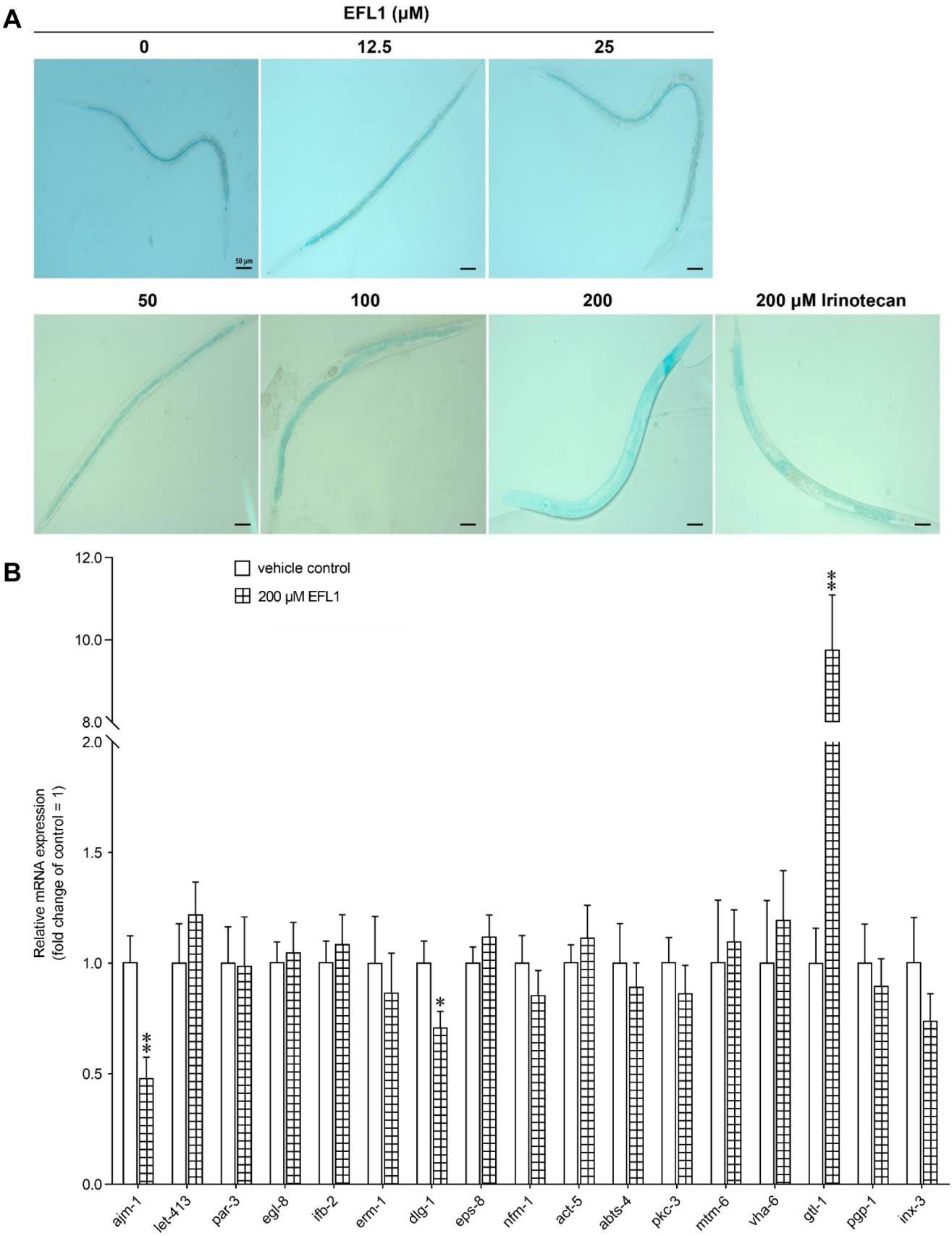

Fig. 5. Effects of EFL1 exposure on the intestinal permeability in *C. elegans*. (A) Representative images of the *C. elegans* showing the dye leakage from the intestinal lumen into the body cavity. The scale bar was 50 μm. (B) Expression pattern comparison of genes required for intestinal development in control and EFL1 exposed groups, the results were expressed as the relative expression *ratio* between targeted genes and tba-1 reference gene. Data were presented as mean ± SEM. of three independent experiments. $^{*}p < 0.05$ or $^{**}p < 0.01$ indicated a statistically significant difference when compared to the control.

Effects of EFL1 on the intestinal permeability of C. elegans

A non-absorbable blue food dye was used to measure the integrity of intestinal barrier. In the vehicle control group, the blue dye was mainly deposited within the intestinal lumen of *C. elegans* (Fig. 5A). In the positive control group, namely 200 μM irinotecan group, the blue dye was leaked from the intestinal lumen into the intestinal cells and body cavity of *C. elegans*, and the leakage was also observed in the 50, 100 and 200 μM EFL1 groups.

The potential molecular mechanism related to the intestinal hyper-permeability was explored by the changes of gene expression levels. In 200 μM EFL1 group, the expression levels of *ajm-1*, and *dlg-1* decreased to 47.83% and 70.67% of control ($p < 0.01$ and $p < 0.05$, respectively), and *gtl-1* increased to 9.75-fold of control ($p < 0.01$), without alteration of expression pattern of *let-413, par-3, egl-8, ifb-2, erm-1, eps-8, nfm-1, act-5, abts-4, pkc-3, mtm-6, vha-6, pgp-1* and *inx-3* (Fig. 5B). In *C. elegans, ajm-1* encodes ortholog of human apical cell-cell junction protein C9orf172, *dlg-1* encodes ortholog of human discs large homolog (DLG) involves in zonula adherens assembly, and *gtl-1* encodes ortholog of human transient receptor potential cation channel subfamily M (TRPM). The results indicated that EFL1-induced intestinal permeability deficiency may be associated with down-regulated cell junction proteins and disordered cation transport.

Effects of EFL1 on the food intake and defecation behavior of C. elegans

The pharyngeal pumping rate and defecation interval were chosen as endpoints to reflect the food intake ability and defecation behavior of *C. elegans*. As shown in Fig. 6A and B, in the 100 and 200 μM EFL1 groups, the pumping rate decreased from 48.2 of control to 42.2 and 42.0 ($p < 0.01$), and the mean defecation cycle length decreased from 48.62 s of control to 46.63s and 43.18 s ($p < 0.01$). The results indicated that EFL1-exposed groups had a weakening food intake ability, along with accelerating excretion.

In general, genes *unc-13* and *unc-36* involved in the regulation of pharyngeal pumping, and encoded orthologs of human unc-13 homolog A (UNC13A) and calcium voltage-gated channel auxiliary subunit alpha 2 (CACNA2), respectively. But in the present study, both of them were not found to be related to EFL1-induced pumping rate descending (Fig. 6C).

The accelerated defecation rhythm contributed to several genes. In the 200 μM EFL1 group, genes expression levels of *unc-101, shn-1, flr-4,*

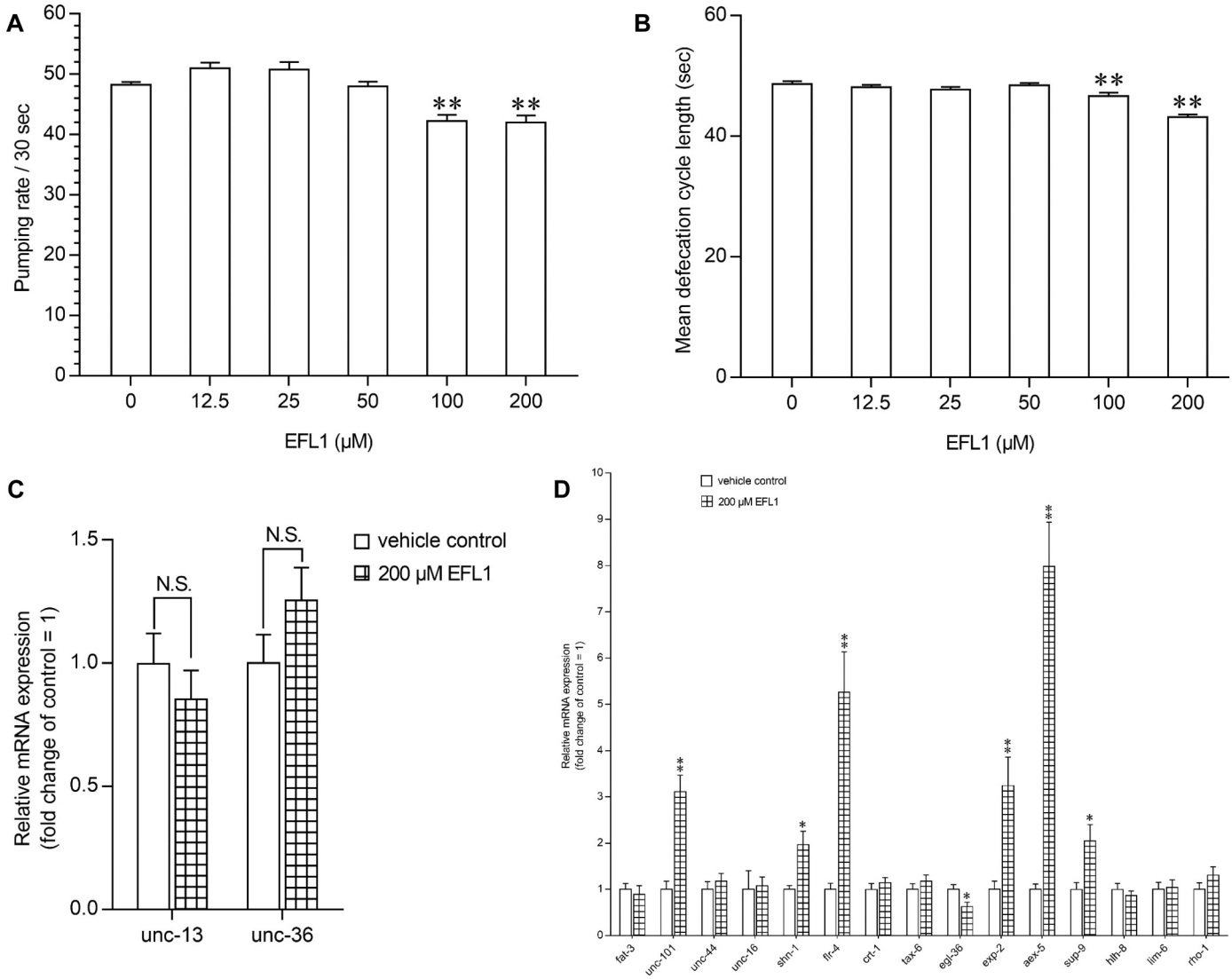

Fig. 6. Effects of EFL1 exposure on the food intake and defecation behavior in *C. elegans*. (A) Effects of EFL1 exposure on pharyngeal pumping rate. (B) Effects of EFL1 exposure on mean defecation cycle length. Expression pattern comparison of genes required for pharyngeal pumping (C) and defecation behavior (D) in control and EFL1 exposed groups, the results were expressed as the relative expression *ratio* between targeted genes and tba-1 reference gene. Data were presented as mean ± SEM. of three independent experiments. *$p < 0.05$ or **$p < 0.01$ indicated a statistically significant difference when compared to the control.

exp-2, aex-5 and *sup-9* increased to 3.11-, 1.97-, 5.26-, 3.24-, 7.98- and 2.05-fold of control, respectively ($p < 0.05$ or $p < 0.01$); *egl-36* decreased to 62.67% of control ($p < 0.05$) (Fig. 6D). EFL1 did not influence the expression pattern of *fat-3, unc-44, unc-16, crt-1, tax-6, hlh-8, lim-6* and *rho-1*. In *C. elegans, unc-101* encodes adaptor protein-1 complex subunit mu-1 (AP1M1) which involves in transport of metabolites; *shn-1* and *flr-4* regulate rhythmic behavior; *egl-36* and *exp-2* regulate ion transmembrane transport; *aex-5* and *sup-9* regulate muscle contraction.

Effects of EFL1 on the ROS accumulation of C. elegans

EFL1 induced oxidative damage in *C. elegans* was evaluated by intestinal ROS accumulation. After exposure for 72 h, DCF fluorescence intensity, representing ROS accumulation, significantly increased to 3.28- and 12.53-fold of control in 100 and 200 μM EFL1 groups ($p < 0.01$) (Fig. 7A and B). In the positive control group, namely 0.03% H_2O_2-exposed group, ROS accumulation increased to 18.31-fold of control ($p < 0.01$). Excessive ROS accumulation in *C. elegans* led to decreased antioxidant defense capacity and resulted in oxidative damage.

The expression levels of genes were measured to find out vital factors involved in EFL1-induced oxidative damage. As shown in Fig. 7C, EFL1 did not alter the expression patterns of *mev-1, isp-1, ctl-2* and *ctl-3* in nematodes, but significantly increased the expression levels of *sod-1, sod-2, sod-3, sod-4, clk-1* and *ctl-1* to 2.45-, 11.48-, 1.26-, 5.06-, 2.02- and 2.24-fold of control, respectively ($p < 0.05$ or $p < 0.01$). In *C. elegans, sod-1* and *sod-4* genes encode orthologs of human copper/zinc-dependent superoxide dismutase (SOD); similarly, *sod-2* and *sod-3* genes encode manganese-dependent SOD, *clk-1* encodes coenzyme Q biosynthesis protein 7 (COQ7), and *ctl-1* encodes catalase (CAT). These results suggested that EFL1-induced oxidative damage may be associated with the alteration of the SOD, COQ7 and CAT.

Effects of EFL1 on the intestinal lipofuscin levels of C. elegans

Intestinal autofluorescence, which is generated by secondary lysosomal and consists primarily of lipid peroxidation products and oxidized proteins resist proteolytic degradation, accumulates over time in postmitotic mammalian cells (Berdichevsky et al., 2010; Boehm and Slack, 2005). In the present study, the relative fluorescent intensity raised along with increasing concentration of EFL1, up to 108.68%, 111.75% and 123.79% of control in 50, 100 and 200 μM EFL1 groups ($p < 0.05$ or $p < 0.01$) (Fig. 8). The results indicated that EFL1 accelerated lipid oxidation and deposition of metabolic wastes in the intestine of *C. elegans*.

Protein structure of UNC-47 and its interaction with EFL1

The structure of UNC-47 was predicted by homologous modeling with a C-score value of −1.11, indicating a confident prediction (Fig. 9A). As shown in Fig. 9B, UNC-47 was a vesicular inhibitory amino acid transporter containing 486 residues, of which the residues numbers of alpha-helix, beta-strand and random coil in the secondary structure were 311, 9 and 166, respectively. The mean normalized B-factor value was −0.33, meaning a stable inherent thermal mobility of residues in UNC-47 structure. The mean estimated local accuracy was 4.95 Å (Fig. 9C).

Molecular docking was carried out to predict the interaction between EFL1 and UNC-47. As shown in Fig. 9D, the active pocket was generated by PyMOL software (Schrödinger, New York, NY, USA). EFL1 could dock into the active pocket with a total score of 8.28, suggesting a

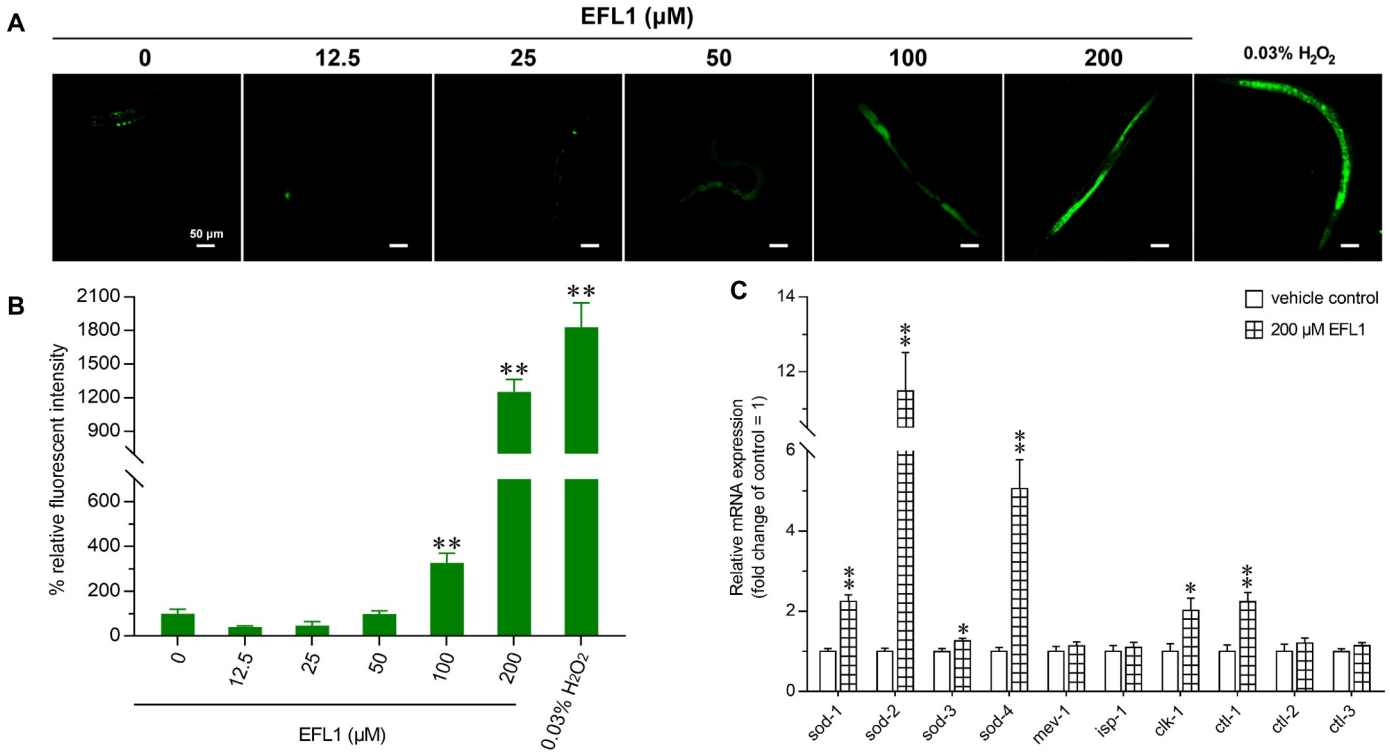

Fig. 7. Effects of EFL1 exposure on the intestinal ROS generation in *C. elegans*. (A) Representative images of the *C. elegans* showing the intestinal ROS generation. The scale bar was 50 μm. (B) Comparison of the relative fluorescent intensity of DCF between the control and EFL1 exposed groups. (C) Expression pattern comparison of genes required for oxidative stress in control and EFL1 exposed groups, the results were expressed as the relative expression *ratio* between targeted genes and *tba-1* reference gene. Data were presented as mean ± SEM. of three independent experiments. *$p < 0.05$ or **$p < 0.01$ indicated a statistically significant difference when compared to the control.

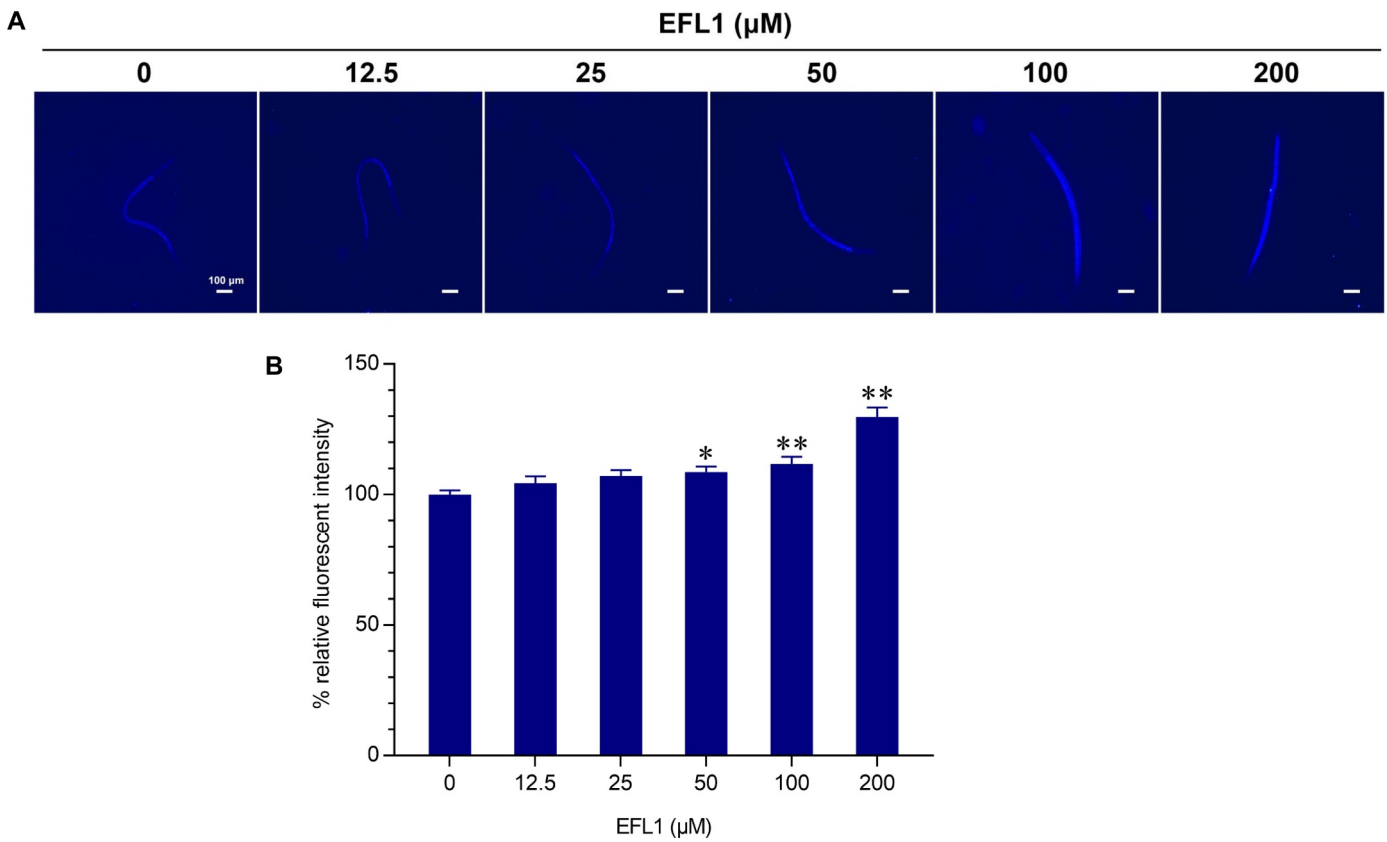

Fig. 8. Effects of EFL1 exposure on intestinal lipofuscin accumulation in *C. elegans*. (A) Representative images of the *C. elegans* showing the accumulation of autofluorescent lipofuscin in the intestinal cells. The scale bar was 100 μm. (B) Comparison of the relative fluorescent intensity between the control and EFL1 exposed groups. Data were presented as mean ± SEM. of three independent experiments. $*p < 0.05$ or $**p < 0.01$ indicated a statistically significant difference when compared to the control.

stable interaction (Fig. 9E). Theoretically, EFL1 bound UNC-47 *via* the formation of one hydrogen bond at Asn231, two hydrogen bonds at Lys351, and nine hydrophobic contacts with Ala101, Leu177, Thr180, Leu227, Ser228, Thr279, Phe283, Pro359 and Ala363 (Fig. 9F).

Effects of EFL1 on GABAergic-related biological factors of C. elegans

To further explore the molecular mechanism of EFL1-accelerated defecation rhythm, the present study used green fluorescent protein (GFP)-tagged GABAergic neurons of transgenic strain of *oxIs*12[Ex (P*unc-47::GFP*)], and measured the relative fluorescent puncta size of AVL and DVB after exposed to EFL1. As shown in Fig. 10A and B, the relative size of AVL and DVB respectively decreased to 44.37% and 57.62% of control in 200 μM EFL1 group ($p < 0.01$). In other words, EFL1 suppressed the expression of GFP-tagged protein UNC-47.

The expression levels of genes involved in GABA neurotransmitter were quantified by RT-qPCR. After exposed to 200 μM EFL1, the *gat-1, unc-25* and *unc-33* decreased to 49.67%, 53.83% and 36.50% of control ($p < 0.05$); but *cab-1* and *aex-3* were not altered (Fig. 10C). *gat-1* encodes Na^+/Cl^--dependent GABA transporter 1, *unc-25* and *unc-33* respectively encode orthologs of human glutamate decarboxylase 2 (GAD2) and neural proliferation differentiation and control protein 1(NPDC1), and both involve in GABAergic synaptic transmission. The results suggested that EFL1-accelerated defecation behavior was associated with damaged AVL and DVB neurons, and transport of GABA.

Discussion

In *C. elegans*, several main biological processes and signal transduction, including survival, redox, aging and neurodegenerative disease are similar with humans (Hulme and Whitesides, 2011). Although toxicologists have advocated the application of *C. elegans* model over decades, few studies chose it for the intestinal toxicity assessment *in vivo*. The intestine is one of the major organs of *C. elegans*, and the advantages for intestinal toxicity researches are its transparency, nearly invariant intestinal cell number and development process. Transparency enables studies in living worms utilizing dye or GFP to visualize labeling targets (Kaletta and Hengartner, 2006). In adult worms, the intestine is composed of 20 large epithelial cells positioned as bilaterally symmetric pairs and form a long tube around lumen, and intestine fills the entire body cavity behind the pharynx. In the present study, we tried to assess the intestinal toxicity of EFL1 using *C. elegans*.

After 72 h exposure, 200 μM EFL1 did not cause lethality in *C. elegans*, but body length and body width were inhibited in a concentration dependent manner, so the growth status was a sensitive endpoint of EFL1 toxicity.

The general toxicity of EFL1 were assessed by locomotion capacity and chemoreception behavior. The *C. elegans* moves in a sinusoidal style *via* alternative ventral and dorsal muscle contraction (Zeng et al., 2017). EFL1 accelerated the locomotion behavior represented by frequencies of head thrash and body bend, which are associated with active calcium voltage-gated channel and guanine nucleotide exchange factor (GEF). Overreliance Ca^{2+} may be released from intracellular stores of depolarization, leading to motorial neuron activation. GEF regulate guanosine triphosphatase activity by catalyzing the exchange of guanosine diphosphate for guanosine triphosphate, contributing to energy supply (Marston et al., 2019). In *C. elegans*, two polymodal ASH sensory neurons release glutamate to escape aversive stimulatory signals. In the present study, EFL1 decreased the avoidance index of *C. elegans*, attributing to the down-regulated gene expression of *egl-30*.

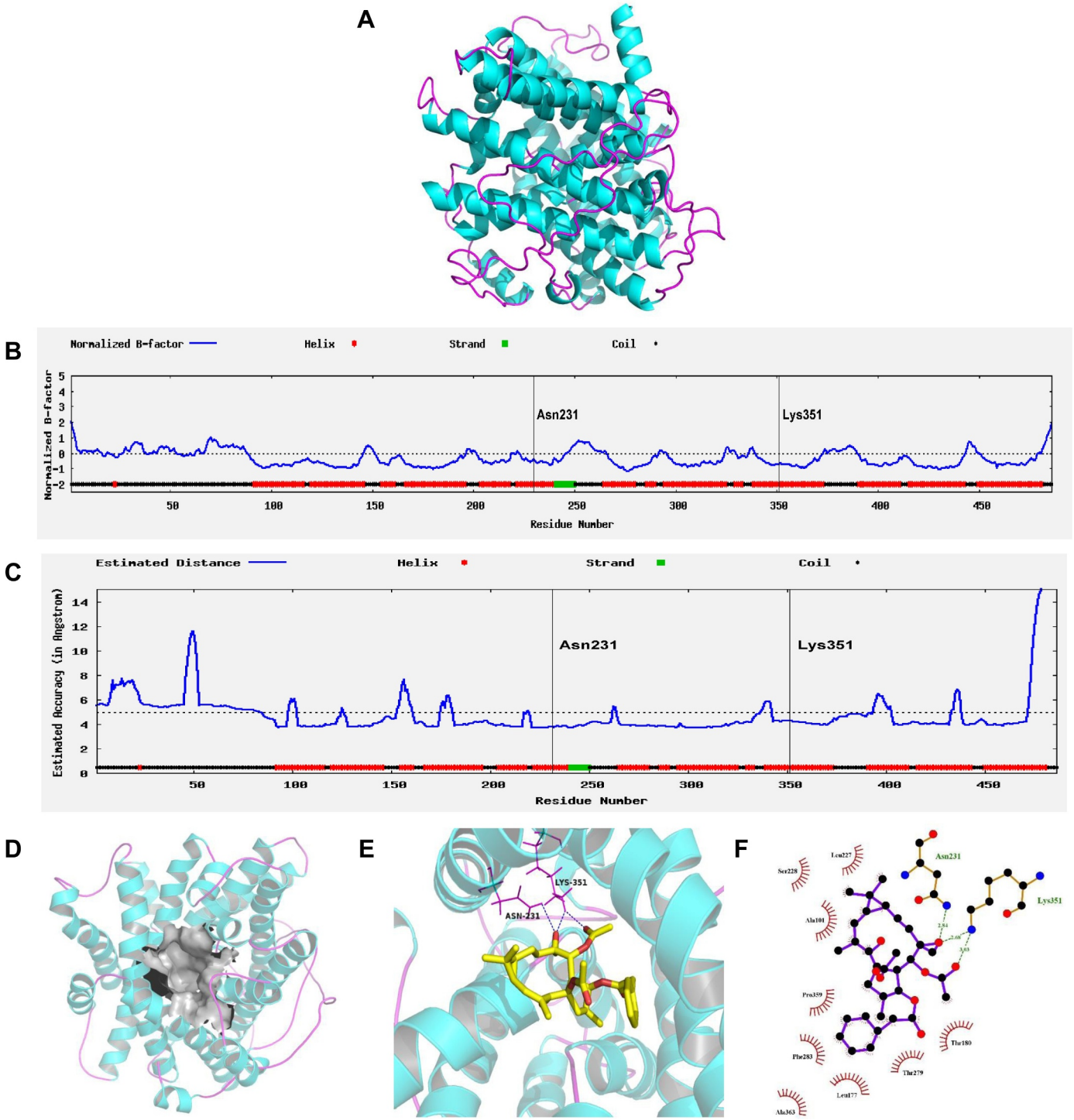

Fig. 9. The homology modeling of UNC-47 protein of *C. elegans*, and molecular docking between UNC-47 and EFL1. (A) The three dimensions (3D) protein structure of UNC-47 predicted by I-TASSER server. (B) The predicted normalized B-factor to assess the extent of the inherent thermal mobility of residues in protein. (C) The estimated accuracy to assess the local structure error of the model. (D) The binding pocket for molecular docking. Molecular interactions between UNC-47 and EFL1. 3D (E) and 2D (F) interaction models were presented.

This gene regulated G protein signaling to promote Ca^{2+} influx and subsequent glutamate release, thus involved in avoidance response to chemical stimuli (Esposito et al., 2010). In EFL1-accelerated locomotion study, calcium voltage-gated channel was active. In EFL1-inhibited chemoreception, Ca^{2+} influx, which controlled glutamate release, was decreased due to the down-regulated *egl-30* gene expression level. The above study indicated that Ca^{2+} signal was multifaceted, and played major role in both locomotion and chemoreception.

Following oral exposure of EFL1, intestine is the primary target organ to deal with xenobiotics, so we investigated whether EFL1 destroyed the integrity of the intestinal barrier, which is indispensable to protect secondary target organs such as muscle and neuron from absorbed toxicants. Recent studies have reported that EFL1 disturbed the immune response and development process of mice intestine, of which interleukin, nuclear factor kappa B, angiopoietin/Tie2 and Janus kinases/signal transducer and activator of transcription pathways were

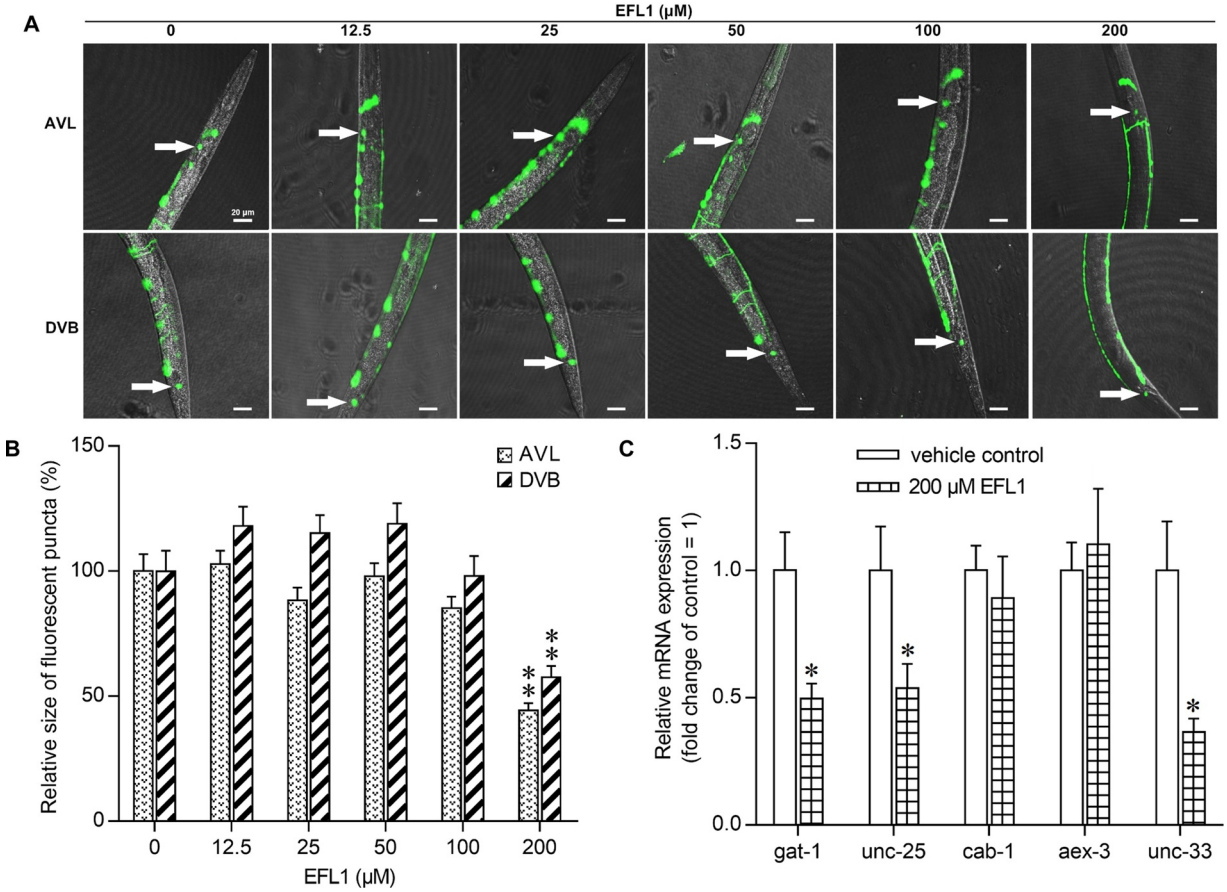

Fig. 10. Effects of EFL1 exposure on GABAergic neurons in *C. elegans*. (A) Representative images of the *C. elegans* showing GFP-tagged AVL and DVB neurons in control and EFL1 exposed groups. The scale bar was 20 μm. (B) Comparison of the relative size of fluorescent puncta of AVL and DVB neurons between the control and EFL1 exposed groups. (C) Expression pattern comparison of genes required for GABA in control and EFL1 exposed groups, the results were expressed as the relative expression *ratio* between targeted genes and tba-1 reference gene. Data were presented as mean ± SEM. of three independent experiments. $^{*}p < 0.05$ or $^{**}p < 0.01$ indicated a statistically significant difference when compared to the control.

highly activated, indicating intestinal inflammation and mucosal barrier impairment (Zhang et al., 2018). In the present study, EFL1 influenced the intestinal permeability of *C. elegans*, and facilitated toxicants leakage from intestinal tract to body cavity. This process was concerned with impaired cell-cell junction and adherens assembly, leading to immoderate transportation of biomacromolecules. Hyper-permeability status was also related to abnormal expressed GTL-1, a ubiquitously expressed ion channel required for Mn^{2+}, Mg^{2+} and Zn^{2+} transportation.

The EFL1-induced intestinal toxicity was also characterized by accelerated defecation behavior in *C. elegans*. Defecation is a rhythmic behavior with a cycle period of 50 s, and consists of three steps of muscle contraction, including posterior body contraction (pBoc), anterior body contraction (aBoc) and enteric muscle contraction (Emc) (Ruan et al., 2016). During Emc, release of GABA from AVL and DVB induces intestinal muscles and anal depressor to contract, and anus will be opened to expel intestinal contents. In this study, EFL1 up-regulated rhythm-related *shn-1* and *flr-4*, as well as muscle contraction-related *aex-5* and *sup-9*. Through molecular docking, we also observed excellent docking scores, hydrogen bonds, and hydrophobic contacts between EFL1 and UNC-47, and the stable interaction indicated that EFL1 could directly affect GABA transportation. The AVL and DBV size, along with expression of GABAergic genes *gat-1, unc-25* and *unc-33* were decreased, suggesting impaired GABA biosynthesis and transportation. The defective GABA-conducted Emc negatively regulated defecation behavior, but enhanced muscle contraction may compensate this damage, and ultimately presented accelerated defecation cycle.

During intestinal impairment process, stress response may be activated in *C. elegans*. The detailed responses of EFL1-induced oxidative damage were evaluated through the analysis of intestinal ROS and lipofuscin accumulation and relevant genes expression levels in *C. elegans*. Despite oxygen is essential for aerobic respiration and energy production to maintain the survival of multicellular organisms including *C. elegans*, it is also harmful after conversion into ROS (Miranda-Vizuete and Veal, 2017). Excessive ROS cause peroxidation of lipid, and lead to irreversible lipofuscin stacking in intestine. In the present study, EFL1 induced intestinal oxidative damage represented by ROS and lipofuscin accumulation. As a compensation to deal with redox imbalance, SOD, CAT and CLK-1 were increased to exert antioxidation activity.

EFL1 was the main toxic ingredient of *Euphorbia* semen-induced diarrhea. The present study elucidated the intestinal toxicity effects and underlying mechanisms of EFL1. Overall, EFL1 destroyed the intestinal barrier *via* down-regulated cell junctions and active cation transport channel, thus allowing intestinal contents leaked to secondary organs like muscles and neurons. The intestinal toxicity effects was also reflected as accelerated defecation behavior, due to the disorder vesicular and ion transport, quickening rhythm regulation, enhanced muscle contraction and injured GABAergic neurons. The oxidative damage represented by ROS and lipofuscin accumulation, as well as unbalanced antioxidant system also involved in the EFL1-induced intestinal toxicity.

The major limitation of the present study was that *C. elegans* lack mammalian organ such as liver. Hence EFL1 in *C. elegans* could not

transform into secondary metabolites. Actually, EFL1 was transformed into secondary metabolites including drolysed esterase, oxydic methyl and methylated hydroxyl *via* hepatic phase I metabolism (Zhu et al., 2018). In the present study, the general and intestinal toxicity observed could account for the parent compound of EFL1.

Conclusion

In the present study, the intestinal toxicity induced by EFL1 was investigated in coelomic model organism *C. elegans*, and characterized by leaky intestinal barrier and accelerated defecation behavior. The underlying mechanisms were related to intestinal oxidative damage, disorder transportation, down-regulated cell junctions, enhanced rhythm behavior and muscle contraction, as well as injured GABAergic neurons. This study provided intestinal toxicity data based on *C. elegans* model for the safety assessment of EFL1.

Declaration of Competing Interest

We wish to confirm that there are no known conflicts of interest associated with this publication and there has been no significant financial support for this work that could have influenced its outcome.

Acknowledgments

The research was financially supported by National Key Research and Development Program of China (No. 2018YFC1704506, 2018YFC1603102, 2018YFC1602705) and National Natural Science Foundation of China (No. 81673685).

References

Bargmann, C.I., Horvitz, H.R., 1991. Chemosensory neurons with overlapping functions direct chemotaxis to multiple chemicals in *C. elegans*. Neuron 7, 729–742.
Berdichevsky, A., Nedelcu, S., Boulias, K., Bishop, N.A., Guarente, L., Horvitz, H.R., 2010. 3-Ketoacyl thiolase delays aging of *Caenorhabditis elegans* and is required for lifespan extension mediated by sir-2.1. Proc. Natl. Acad. Sci. USA 107, 18927–18932.
Boehm, M., Slack, F., 2005. A developmental timing microRNA and its target regulate life span in *C. elegans*. Science 310, 1954–1957.
Brenner, S., 1974. The genetics of *Caenorhabditis* elegans. Genetics 77, 71–94.
Donkin, S.G., Williams, P.L., 1995. Influence of developmental stage, salts and food presence on various end points using *Caenorhabditis elegans* for aquatic toxicity testing. Environ. Toxicol. Chem. 14, 2139–2147.
Esposito, G., Amoroso, M.R., Bergamasco, C., Di Schiavi, E., Bazzicalupo, P., 2010. The G protein regulators EGL-10 and EAT-16, the Giα GOA-1 and the G(q)α EGL-30 modulate the response of the *C. elegans* ASH polymodal nociceptive sensory neurons to repellents. BMC Biol. 8, 138.
Gao, S., Liu, H.Y., Wang, Y.H., He, H.P., Wang, J.S., Di, Y.T., Li, C.S., Fang, X., Hao, X.J., 2007. Lathyranone A: a diterpenoid possessing an unprecedented skeleton from *Euphorbia lathyris*. Org. Lett. 9, 3453–3455.
Gelino, S., Chang, J.T., Kumsta, C., She, X., Davis, A., Nguyen, C., Panowski, S., Hansen, M., 2016. Intestinal autophagy improves healthspan and longevity in *C. elegans* during dietary restriction. PLoS Genet 12, e1006135.
Harris, T.W., Chen, N., Cunningham, F., Tello-Ruiz, M., Antoshechkin, I., Bastiani, C., Bieri, T., Blasiar, D., Bradnam, K., Chan, J., Chen, C.K., Chen, W.J., Davis, P., Kenny, E., Kishore, R., Lawson, D., Lee, R., Muller, H.M., Nakamura, C., Ozersky, P., Petcherski, A., Rogers, A., Sabo, A., Schwarz, E.M., Van Auken, K., Wang, Q., Durbin, R., Spieth, J., Sternberg, P.W., Stein, L.D., 2004. WormBase: a multi-species resource for nematode biology and genomics. Nucleic Acids Res. 32, D411–D417.
Hulme, S.E., Whitesides, G.M., 2011. Chemistry and the worm: *Caenorhabditis elegans* as a platform for integrating chemical and biological research. Angew. Chem. Int. Ed. Engl. 50, 4774–4807.
Jazwinski, S.M., 1996. Longevity, genes, and aging. Science 273, 54–59.
Ji, Z.H., Gao, S., Li, G.J., Wang, Q., 2019. Effects of mercury sulfide on the growth and development in *C. elegans* feeded by inactivated OP50. J. Toxicol. 33, 1–6.
Kaletta, T., Hengartner, M.O., 2006. Finding function in novel targets: *C. elegans* as a model organism. Nat. Rev. Drug Discov. 5, 387–398.
Mahoney, T.R., Luo, S., Round, E.K., Brauner, M., Gottschalk, A., Thomas, J.H., Nonet, M.L., 2008. Intestinal signaling to GABAergic neurons regulates a rhythmic behavior in *Caenorhabditis elegans*. Proc. Natl. Acad. Sci. USA 105, 16350–16355.
Marston, D.J., Anderson, K.L., Swift, M.F., Rougie, M., Page, C., Hahn, K.M., Volkmann, N., Hanein, D., 2019. High Rac1 activity is functionally translated into cytosolic structures with unique nanoscale cytoskeletal architecture. Proc. Natl. Acad. Sci. USA 116, 1267–1272.
Miranda-Vizuete, A., Veal, E.A., 2017. *Caenorhabditis elegans* as a model for understanding ROS function in physiology and disease. Redox Biol. 11, 708–714.
Ruan, Q., Qiao, Y., Zhao, Y., Xu, Y., Wang, M., Duan, J., Wang, D., 2016. Beneficial effects of *Glycyrrhizae radix* extract in preventing oxidative damage and extending the lifespan of *Caenorhabditis elegans*. J. Ethnopharmacol. 177, 101–110.
Schmittgen, T.D., Livak, K.J., 2008. Analyzing real-time PCR data by the comparative C(T) method. Nat. Protoc. 3, 1101–1108.
Spence, A.M., Malone, K.M.B., Novak, M.M.A., Woods, R.A., 1982. The effects of mebendazole on the growth and development of *Caenorhabditis elegans*. Can. J. Zool. 60, 2616–2623.
Wang, D.Y., 2019. Target organ toxicology in *Caenorhabditis elegans*. In: Wang, D.Y. (Ed.), ASH Sensory Neurons. Springer, Singapore, pp. 30–34.
Wang, Y.Z., Zhang, X.T., Li, S.J., Zhang, Y., Li, F.Y., Zhang, C.N., Wang, Q., Li, W.H., Luo, S.X., 2018. Expression of AQP2, AQP4 and AQP8 in mouse intestine induced by unprocessed and processed *Euphorbia lathyris*. Pak. J. Pharm. Sci. 31, 1229–1235.
Wu, Q., Yin, L., Li, X., Tang, M., Zhang, T., Wang, D., 2013. Contributions of altered permeability of intestinal barrier and defecation behavior to toxicity formation from graphene oxide in nematode *Caenorhabditis elegans*. Nanoscale 5, 9934–9943.
Wu, T., He, K., Zhan, Q., Ang, S., Ying, J., Zhang, S., Zhang, T., Xue, Y., Tang, M., 2015. MPA-capped CDTE quantum dots exposure causes neurotoxic effects in nematode *Caenorhabditis elegans* by affecting the transporters and receptors of glutamate, serotonin and dopamine at the genetic level, or by increasing ROS, or both. Nanoscale 7, 20460–20473.
Xia, M., Huang, R., Shi, Q., Boyd, W.A., Zhao, J., Sun, N., Rice, J.R., Dunlap, P.E., Hackstadt, A.J., Bridge, M.F., Smith, M.V., Dai, S., Zheng, W., Chu, P.H., Gerhold, D., Witt, K.L., DeVito, M., Freedman, J.H., Austin, C.P., Houck, K.A., Thomas, R.S., Paules, R.S., Tice, R.R., Simeonov, A., 2018. Comprehensive analyses and prioritization of Tox21 10k chemicals affecting mitochondrial function by in-depth mechanistic studies. Environ. Health Perspect. 126, 077010.
Yang, J., Wang, Y., Zhang, Y., 2016. ResQ: an approach to unified estimation of B-factor and residue-specific error in protein structure prediction. J. Mol. Biol. 428, 693–701.
Yang, J., Yan, R., Roy, A., Xu, D., Poisson, J., Zhang, Y., 2015. The I-TASSER suite: protein structure and function prediction. Nat. Methods 12, 7–8.
Zeng, R., Yu, X., Tan, X., Ye, S., Ding, Z., 2017. Deltamethrin affects the expression of voltage-gated calcium channel α1 subunits and the locomotion, egg-laying, foraging behavior of *Caenorhabditis elegans*. Pestic. Biochem. Physiol. 138, 84–90.
Zhang, C.Y., Wu, Y.L., Zhang, P., Chen, Z.Z., Li, H., Chen, L.X., 2019. Anti-inflammatory lathyrane diterpenoids from *Euphorbia lathyris*. J. Nat. Prod. 82, 756–764.
Zhang, J.Y., Mi, Y.J., Chen, S.P., Wang, F., Liang, Y.J., Zheng, L.S., Shi, C.J., Tao, L.Y., Chen, L.M., Chen, H.B., Fu, L.W., 2011. *Euphorbia* factor L1 reverses ABCB1-mediated multidrug resistance involving interaction with ABCB1 independent of ABCB1 downregualtion. J. Cell. Biochem. 112, 1076–1083.
Zhang, Y., Wang, Y., Li, S., Zhang, X., Li, W., Luo, S., Sun, Z., Nie, R., 2018. ITRAQ-based quantitative proteomic analysis of processed *Euphorbia lathyris* L. for reducing the intestinal toxicity. Proteome Sci. 16, 8.
Zhao, Y., Zhi, L., Wu, Q., Yu, Y., Sun, Q., Wang, D., 2016. p38 MAPK-SKN-1/Nrf signaling cascade is required for intestinal barrier against graphene oxide toxicity in *Caenorhabditis elegans*. Nanotoxicology 10, 1469–1479.
Zhu, A., Sun, Y.Q., Zhong, Q.W., Yang, J.L., Zhang, T., Zhao, J.W., Wang, Q., 2019. Effect of *Euphorbia* factor L1 on oxidative stress, apoptosis and autophagy in human gastric epithelial cells. Phytomedicine 64, 152929.
Zhu, A., Zhang, T., Wang, Q., 2018. The phytochemistry, pharmacokinetics, pharmacology and toxicity of *Euphorbia* semen. J. Ethnopharmacol. 227, 41–55.